AGU PUBLICATIONS

Water Resources Research

RESEARCH ARTICLE
10.1002/2016WR018832

Key Points:
- Seven tracer injections over 28 h analyzed using rank Storage Selection function theory of time-varying transit time distributions
- rSAS results show fluctuations in turnover rate of reach storage at base flow limited to a volume 5 times larger than visible channel
- Method suggests an approach to parsimonious reach-scale solute transport that accounts for time-varying stream-hyporheic exchange dynamics

Correspondence to:
C. J. Harman,
charman1@jhu.edu

Citation:
Harman, C. J., A. S. Ward, and A. Ball (2016), How does reach-scale stream-hyporheic transport vary with discharge? Insights from rSAS analysis of sequential tracer injections in a headwater mountain stream, *Water Resour. Res.*, *52*, doi:10.1002/2016WR018832.

Received 25 FEB 2016
Accepted 2 AUG 2016
Accepted article online 5 AUG 2016

How does reach-scale stream-hyporheic transport vary with discharge? Insights from rSAS analysis of sequential tracer injections in a headwater mountain stream

C. J. Harman[1], A. S. Ward[2], and A. Ball[1]

[1]Department of Geography and Environmental Engineering, Johns Hopkins University, Baltimore, Maryland, USA, [2]School of Public and Environmental Affairs, Indiana University, Bloomington, Indiana, USA

Abstract The models of stream reach hyporheic exchange that are typically used to interpret tracer data assume steady-flow conditions and impose further assumptions about transport processes on the interpretation of the data. Here we show how rank Storage Selection (rSAS) functions can be used to extract "process-agnostic" information from tracer breakthrough curves about the time-varying turnover of reach storage. A sequence of seven slug injections was introduced to a small stream at base flow over the course of a diel fluctuation in stream discharge, providing breakthrough curves at discharges ranging from 0.7 to 1.2 L/s. Shifted gamma distributions, each with three parameters varying stepwise in time, were used to model the rSAS function and calibrated to reproduce each breakthrough curve with Nash-Sutcliffe efficiencies in excess of 0.99. Variations in the fitted parameters over time suggested that storage within the reach does not uniformly increase its turnover rate when discharge increases. Rather, changes in transit time are driven by both changes in the average rate of turnover (external variability) and changes in the relative rate that younger and older water contribute to discharge (internal variability). Specifically, at higher discharge, the turnover rate increased for the youngest part of the storage (corresponding to approximately 5 times the volume of the channel), while discharge from the older part of the storage remained steady, or declined slightly. The method is shown to be extensible as a new approach to modeling reach-scale solute transport that accounts for the time-varying, discharge-dependent turnover of reach storage.

1. Introduction

Hyporheic exchange is known to be mechanistically coupled to the hydrological controls of stream discharge and near-stream hydraulic gradients. However, the most common method used to characterize hyporheic exchange—the analysis of solute tracer breakthrough curves—has failed to identify consistent controls on hyporheic exchange under time-variable hydrologic conditions [e.g., *Ward et al*., 2013a; *Payn et al*., 2009]. To-date, time-variable hyporheic exchange has been reported in response to variable base flow conditions [*Ward et al*., 2012; *Payn et al*., 2009; *Ward et al*., 2013b], diel fluctuations in discharge [*Loheide and Lundquist*, 2009; *Sawyer and Cardenas*, 2009; *Sawyer et al*., 2013; *Wondzell et al*., 2009a], and storm event responses [*Ward et al*., 2013a; *Malzone and Lowry*, 2014; *Schmadel et al*., 2016]. Several studies that include high replication in space or through storm events report that observed variations in reach-scale tracer transport and inferred hyporheic exchange could not be explained by discharge alone [*Wondzell*, 2006; *Ward et al*., 2012; *Payn et al*., 2009; *Ward et al*., 2013b]. As such, it remains unknown if observed variations in hyporheic exchange and reach-scale transport arise because of variations in stream discharge, changes in hyporheic flow paths themselves, or a combination of the two.

This confusion may be, in part, a result of limitations in the methods used to interpret solute tracer studies—in particular, their ability to account for transient hydrological dynamics. Recent work has demonstrated that transport variability in response to dynamic hydrologic forcing can be decomposed into two distinct components, termed *external* and *internal* variability [*Kim et al*., 2016]. Both types might contribute to overall transport variability of a given system, though one may dominate over the other. Neither is well represented in most of the methods used to interpret tracer breakthrough curves.

A more detailed discussion of these concepts is provided in *Kim et al*. [2016], but they can be understood intuitively for the case were a hydrodynamic system can be reduced to a set of streamtubes, or more loosely

as a set of flow pathways. External variability refers to changes in the overall flow rate through set of all flow pathways, without implying any change in the proportion of flow through one flow pathway relative to another. If all variability is external, the velocity along all flow paths increases proportionally to accommodate an increase in flow. The ratio of the flux rate along any two flow paths remains constant. Internal variability implies that the flow through some parts of the system increases (or decreases) by a different proportion than through other parts. The velocity field has changed in some way other than a proportional scaling. This reorganization of relative flow magnitudes may arise from a fluctuation in the potentiometric field around a stream or changing interactions between streams and their catchments [*Harvey and Bencala*, 1993; *Ward et al*., 2016]. However, in most hydrologic systems (with the possible exception of a confined aquifer), a change in flow through the system will induce both internal and external variability. If we can quantify these two contributions, we can ask: what are the relative contributions of each? and what does the structure of the internal variability tell us about the changing structure of the flow paths?

Common methods for analyzing tracer data and modeling stream reaches typically assume steady flow, and even those that allow for variable flow in-channel assume steady flow through the transient storage zones. In all cases, models are subject to two primary limitations. First, models are based on conceptual representations of the real system and necessarily reduce complexity. The most common approaches [*Bencala and Walters*, 1983; *Haggerty et al*., 2000; *Worman et al*., 2002] use inverse modeling to fit experimental results, analyzing the best fit parameter set to represent the dominant processes in the stream-hyporheic system. While adding processes may improve fit [*Briggs et al*., 2009; *Kerr et al*., 2013; *Choi et al*., 2000], the addition of processes and parameters increases the field observations required to parameterize the model and may increase existing problems with parameter interaction and/or uncertainty [*Wagner and Harvey*, 1997; *Kelleher et al*., 2013]. Second, stream transport models commonly require a static and spatially homogeneous transit time distribution for storage locations. Steady flow is assumed, implicitly or explicitly, whenever tracer breakthrough curves are interpreted in terms of a fixed transit time distribution. *Runkel et al*. [1998] coupled an unsteady flow model with the transient storage model, dynamically adjusting stream area and advection with discharge but fixing other parameters describing exchange between the stream and hyporheic zone. Still, this approach remains uncommon and experimentalists may lack data to describe the time-variable parameter relationships. Other techniques such as the concept of "flow-weighted time" may be applied [e.g., *Rodhe et al*., 1996], but have not been broadly attempted in studies of stream-hyporheic exchange.

Overall, existing methods fail to address the deeper "process" issue: the flow paths themselves are likely to change in response to changes in discharge—i.e., changes in discharge will induce external *and* internal variability. As such, the transit time distribution will be time-varying even in flow-weighted time [*Kim et al*., 2016]. This limitation cannot be addressed by simply allowing the shape of the assumed transit time distributions to change in time, as this will lead to mass balance errors [*Botter et al*., 2010; *Harman*, 2015]. It is therefore important to better understand how internal variability is linked to stream discharge. Discharge is commonly viewed a master variable in stream corridors, linked to predictable patterns in ecosystem function [*Vannote et al*., 1980; *Stanford and Ward*, 1993], geomorphology [*Leopold and Maddock*, 1953], and solute transport [*Gooseff et al*., 2008; *Fischer et al*., 1979]. However, the internal variability of hyporheic zones has received limited study, because subsurface observations are difficult to make in the field [*Bencala et al*., 2011]. Still, several recent studies demonstrate apparent internal variability in hyporheic zones, observing apparent flow path-scale responses to hydrologic dynamics [*Voltz et al*., 2013; *Dudley-Southern and Binley*, 2015].

The concept of a *rank* Storage Selection (or rSAS) function provides an alternative approach to breakthrough curve analysis that separates the influence of internal and external variability, allowing their relative influence on transport to be examined. This approach was developed and applied initially for catchment-scale applications [*Harman*, 2015] and has not yet been applied to reach-scale studies of stream-hyporheic systems. The rSAS theory is a generalization of the theory of transit time distributions to fully time-variable conditions. The transit time distribution is not fit to the breakthrough curve directly [e.g., *Kirchner et al*., 2000]. Instead, a pdf is selected for the rSAS function, and this is combined with the time-varying flow to yield a time-varying transit time distribution. The parameters of the rSAS function can be chosen to best reproduce the observed data. Unlike the transit time distribution, the rSAS function only varies in time when there is internal variability.

The objective of this study is to examine time-variable transport in a stream-hyporheic system in the context of internal and external variability. We take the well-studied Watershed 1 (WS01) at the H.J. Andrews Experimental Forest as a test-case to assess the relative roles of internal and external variability in explaining stream-hyporheic observations. Using existing studies, it is possible to formulate (apparently) contradictory hypotheses that emphasize the role of either internal or external variability:

H1: Internal variability is the dominant control on stream-hyporheic exchange. Stream solute tracer studies in WS01 demonstrate time-variable transport at the reach scale through base flow recession and storm events [*Wondzell et al*., 2007, 2009a; *Ward et al*., 2013a]. Based on in-stream tracer observations, past efforts conclude that discharge alone (i.e., external variability) is not sufficient to explain in-stream solute tracer observations [*Ward et al*., 2013a]. As such, internal variability has been invoked as a possible explanatory mechanism [*Ward et al*., 2013a]. Indeed, *Voltz et al*. [2013] report time-variable hydraulic gradients in the valley bottom, a likely indicator of spatial reorganization of hyporheic flow paths (i.e., internal variability). Furthermore, *Ward et al*. [2016] found time-variable hyporheic transport through base flow recession at monitoring wells distal from the stream itself. Because conceptual models have invoked internal variability to explain observations [*Ward et al*., 2013a,], and because internal variability has been observed [*Voltz et al*., 2013; *Ward et al*., 2016], *internal variability* can be hypothesized to be the dominant control on stream-hyporheic exchange in WS01.

H2: External variability is the dominant control on stream-hyporheic exchange. More recently, *Ward et al*. [2016] analyzed direct subsurface observations to assess internal variability through base flow recession. They found that the behavior of flow paths near the stream is dominated by hydrostatic gradients around pool-riffle-step structures, and was minimally variable through base flow recession (i.e., no internal variability for these flow paths); only more distal flow paths exhibited variation in their time scales. Because stream solute tracers are known to be primarily sensitive to the shortest and fastest hyporheic flow paths (commonly the "window of detection," in the sense of *Harvey et al*. [1996]), and because these shortest and fastest flow paths were observed to be time-invariant [*Ward et al*., 2016], *external variability* can be hypothesized to be the dominant control on stream-hyporheic exchange in WS01.

To test these hypotheses, we conducted a series of solute tracer injections during a period of changing streamflow conditions in WS01. By applying the rSAS approach to the experimental data set, we estimate the relative role of internal and external variability in yielding the observed transport in the stream. Furthermore, this approach allows us to relate changes in hydrologic forcing to changes in the Storage Selection function, suggesting an approach to forward modeling of stream reach transport.

2. Background

2.1. Rank Storage Selection (rSAS) Theory

Storage Selection (SAS) theory provides a basis for interpreting tracer data and modeling solute transport through arbitrary control volumes [*Rinaldo et al*., 2015; *Harman*, 2015]. The concept of a *rank* Storage Selection (rSAS) function was presented in *Harman* [2015], and extends previous approaches [*van der Velde et al*., 2012]. An outline of the theory is provided here, with additional developments tailored to the needs of the present work, but full details can be found in the cited papers.

rSAS theory is based on a formal accounting of the "age" of infinitesimal parcels of water in a control volume. The control volume can be of any size, but the fluxes of water across its boundary must be known. (Note that fluxes of water here are calculated in terms of volume, rather than mass, since we assume compressibility is negligible.) Here the control volume will be the stream reach, including its hyporheic and in-channel transient storage zone. We assume that down-valley transport in the hyporheic zone across the reach boundaries is negligible (as many commonly used models do, such as the transient storage model of *Bencala and Walters* [1983]), and that gross inflows and outflows of groundwater are negligible over the study reach (note the possible effects of riparian potential gradients on the structure of the rSAS function will be examined). The rSAS framework could be extended to account for groundwater transport if additional hydrogeologic data were available to quantify these fluxes. The age T of a parcel of water at time t is defined relative to the time t_i that it entered the system with the inflow: $T = t - t_i$. Following the definitions used in previous papers [*Harman*, 2015; *Rinaldo et al*., 2015], $P_S(T,t)$ is the distribution of ages of all water *in storage* at time t (or $p_S(T,t)$ when referring to the probability density function, or pdf). The transit time of a

parcel is the age T of the parcel at the time that it exits as discharge at the downstream end of the reach. The backward transit time distribution $P_Q(T,t)$ (or $p_Q(T,t)$ for the pdf) is the probability distribution representing the transit times T of all the parcels exiting at a particular time t.

In rSAS theory, a new variable is introduced, the *age-ranked storage* S_T (which has units of volume [L^3] or volume normalized by area [L]), representing the volume of water in the control volume with an age less than T at time t. This is simply an unnormalized version of the cumulative distribution of ages in storage (i.e., if total storage S were known, we could calculate $P_S(T,t)=S_T(T,t)/S(t)$). The value of $S_T(T,t)$ associated with a certain age T is the volume of water that has entered *after* time $t-T$, and remains in the system at time t. It can therefore be interpreted as a measure of the progress through storage of the water that entered at time $t-T$. If $S_T(T,t)$ is close to zero, the T-aged water is amongst the youngest in the system. If $S_T(T,t)$ is close to the total storage $S(t)$, it is amongst the oldest.

We can also define a similar variable $Q_T(T,t)$ (units of [$L^3\ T^{-1}$] or [$L\ T^{-1}$]) representing the rate water with an age less than T is leaving the system at time t. This, in turn is simply an unnormalized version of the transit time distribution, so that $P_Q(T,t)=Q_T(T,t)/Q(t)$.

The age-ranked storage S_T can be determined from a conservation of mass law for water less than an age T. This is given by:

$$\frac{d}{dt}S_T(t-t_i,t)=\frac{\partial S_T}{\partial T}+\frac{\partial S_T}{\partial t}=J(t)-Q_T(T,t) \tag{1}$$

The left-hand side of this equation gives the rate of change of the amount of water younger than a certain age T. This is the volume of water that entered the system since time $t-T$ remaining in the system at time t. The right-hand side accounts for controls on this. First, new water flowing into the control volume $J(t)$ (which has units of [$L^3\ T^{-1}$] or [$L\ T^{-1}$]) has age zero, so this adds to S_T. Second, $Q_T(T,t)$ is the rate this water is being removed from the control volume.

Since the function $S_T(T,t)$ maps ages T onto volumes S_T in a monotonically increasing way, it is possible to express the same probability that $P_Q(T,t)$ gives in terms of T, in terms of S_T instead. That is, we can construct a function $\Omega_Q(S_T,t)$ such that $\Omega_Q(S_T,t)=P_Q(T,t)$ when $S_T=S_T(T,t)$. The resulting cumulative distribution function, $\Omega_Q(S_T,t)$, is called the rank Storage Selection (rSAS) function for the discharge. The rSAS function is a probability distribution defined over the total storage in the system. Taking the derivative of the above definition, we find that $p_Q(T,t)=\omega_Q(S_T,t)\partial S_T/\partial T$, where $\omega_Q(S_T,t)$ is the probability density function (pdf) of the rSAS function. That is:

$$p_Q(T,t)\partial T=\omega_Q(S_T,t)\partial S_T \tag{2}$$

for $S_T=S_T(T,t)$. In other words, the fraction of discharge derived from age increment ∂T is equal to the fraction from age-ranked storage increment ∂S_T. That is, $\omega_Q(S_T,t)$ is simply the transit time distribution expressed in terms of storage, rather than age. If the fluxes ($Q(t)$ and $J(t)$) and rSAS function $\Omega_Q(S_T,t)$ are known for all t, the conservation law can be solved to provide the mapping $S_T=S_T(T,t)$ that allows the time-varying transit time distribution $p_Q(T,t)$ to be recovered.

Finally, if the inflow contains a concentration $C_J(t)$ of an ideal conservative tracer, the outflow concentration $C_Q(t)$ is determined by the integral [*Rinaldo et al.*, 2011]:

$$C_Q(t)=\int_{-\infty}^{t}C_J(t_i)p_Q(t-t_i,t)dt_i \tag{3}$$

This integral reduces to a simple convolution for the case of time-invariant p_Q.

2.2. Internal and External Variability

The rSAS function can itself be a time-varying distribution, allowing us to account for changes in the internal transport dynamics of the system, in addition to rigorously accounting for external variability due to the time-variable inflows and outflows. We can examine the nature of internal and external variability revealed by the stream breakthrough curve data by recasting the framework described above in two different ways. First, by taking the derivative of $S_T(T,t)$ with respect to T, we obtain the age-rank storage density $s_T(T,t)$,

which refers to the (infinitesimal) volume of water that entered at time $t-T$ that is still in the system at time t. Once this volume enters it is depleted by the outflows at a rate given by $q_T(T,t)=\partial Q_T/\partial T$. Thus:

$$\frac{d}{dt}s_T(t-t_i,t)=\frac{\partial s_T}{\partial T}+\frac{\partial s_T}{\partial t}=-q_T(T,t) \tag{4}$$

which is simply the derivative of equation (1) with respect to age T.

From the definition $P_Q(T,t)=\Omega_Q(S_T,t)$, it follows that $q_T(T,t)=Q(t)\omega_Q(S_T,t)s_T(T,t)$. This shows that the rate that water of age T is discharged from the system depends on (1) the overall rate of discharge, (2) the location of that water in the overall age-ranked storage $S_T=S_T(T,t)$, and (3) the value of the rSAS function $\omega_Q(S_T,t)$ at that rank in storage at that time.

In the absence of internal variability, the rSAS function is constant in time [*Kim et al.*, 2016], so that $\omega(S_T,t)=\omega(S_T)$. Then $q_T(T,t)$ reduces to $Q(t)\omega_Q(S_T)s_T(T,t)$. Note that the age-ranked storage density $s_T(T,t)$ is still time-variable because the discharge $Q(t)$ is, and hence $p_Q(T,t)$ varies in time. However, water of age rank S_T always represents the same *proportion* of the total discharge. Thus, when the rSAS function is fixed in time, all transport variability is *external* variability, and there is no internal variability.

Conversely, we could fix the flux at a constant rate $J(t)=Q(t)=Q_0$, while allowing the rSAS function to vary, so that the rate is then $q_T(T,t)=Q_0\,\omega(S_T,t)s_T(T,t)$. Then all variability is *internal* with no external variability. Finally, if flow was steady and the rSAS function was fixed, transport would lack either form of variability, and the rate would be a function only of the location of the parcel in age-ranked storage $q_T(T)=Q_0\omega(S_T)s_T(T)$. In that case, s_T (and S_T) would vary only with age and not with time, and the conservation law (equation (1)) reduces to:

$$\frac{ds_T}{dT}=-Q_0\,\omega_Q(S_T(T))) \tag{5}$$

This implies that the transit time distribution is also fixed in time. The equivalent fixed transit time distribution can be found using the definition $P_Q(T)=\Omega(S_T)$, and integrating the conservation equation to obtain the (fixed) value of S_T corresponding to each age T [*Harman*, 2015].

These cases are summarized as follows:

$$q_T=Q(t)\times\omega(S_T,t)\times s_T(T,t)\ \text{ internal and external variability}$$
$$Q(t)\times\omega(S_T)\times s_T(T,t)\ \text{ external variability only}$$
$$Q_0\times\omega(S_T,t)\times s_T(T,t)\ \text{ internal variability only}$$
$$Q_0\times\omega(S_T)\times s_T(T)\ \text{ no variability}$$

In this study, we will assess how the rSAS approach is able to reproduce observed stream tracer dynamics when different combinations of internal and external variability are assumed.

2.3. Dynamics of Storage Turnover

A second way to reformulate this framework can provide further insight into the behavior of storage with different ages. Given an age T, we can (conceptually) divide the water in storage into a part that is younger than T, which is $S_T(T,t)$, and a part that is older than T, which we will call $\overline{S_T}(T,t)$. Note that the sum of these is the total storage:

$$S_T(T,t)+\overline{S_T}(T,t)=S(t) \tag{6}$$

We do not know the total storage of the stream reach, but can estimate the changes in storage relative to some reference state S_{ref} (which may be the initial condition) from conservation of mass. Defining $\Delta S(t)=S(t)-S_{ref}$ and $\Delta\overline{S_T}(T,t)=\overline{S_T}(T,t)-S_{ref}$, we can see that:

$$\Delta\overline{S_T}(T,t)=\Delta S(t)-S_T(T,t) \tag{7}$$

There is an advantage to considering the age-ranked fluxes in terms of $\Delta\overline{S_T}$ rather than S_T in time-variable conditions. Much of the time-variability in hydrologic systems is associated with young water, while the older water moves at a steadier pace [*Harman*, 2015]. Thus, there ought to be a way to quantify the rate

that "old" water is being discharged from the "old" parts of storage. Defining the flux of old water from the system as the complement to the flux of young water, $\overline{Q_T}=Q-Q_T$, we can define a function that describes the rate that old water is being discharged from storage:

$$\overline{Q_T}=F_S(\Delta\overline{S_T},t)=Q(t)(1-\Omega_Q(\Delta S-\Delta\overline{S_T},t)) \tag{8}$$

or alternatively in a density form, to isolate just the flux rate of water along a flow path representing a particular age rank in storage:

$$\frac{\partial\overline{Q_T}}{\partial\overline{S_T}}=f_S(\Delta\overline{S_T},t)=Q(t)\omega_Q(\Delta S-\Delta\overline{S_T},t)) \tag{9}$$

where $f_S=\partial F_S/\partial\Delta\overline{S_T}$.

The advantage of considering variations in $\overline{Q_T}$ (rather than just variations in Ω) is that through it we can understand in an intuitive way how a fluctuation in Q affects the shape of the rSAS function. Consider a hydrologic system in which an increase in total flow through the system (and consequent increase in total storage) is largely accommodated by a higher rate of turnover of the youngest water in the system, while the older water continues to turnover at the same rate. The turnover of the older water $\overline{Q_T}$ (for some $\Delta\overline{S_T}$ corresponding with just the older water) in such a case *will remain fixed in time*. In other words, if we observe that $\overline{Q_T}$ does not vary much for small values of $\Delta\overline{S_T}$ (relative to the variations in total discharge) we can conclude that the variations in the rSAS function are largely the result of changes in the turnover of young water.

We speculate that this scenario is likely true for many typical hydrologic systems, including hyporheic exchange in a stream. Results below will be considered both in terms of S_T, Q_T and $\Delta\overline{S_T}$, $\overline{Q_T}$ to examine this possibility here.

3. Methods

Stream tracer data were analyzed to determine: first, the degree to which internal and external variability control the dynamics of reach-scale transport under varying discharge; second, the way storage of various ages is mobilized, as revealed by the functions F_S and f_s; and third, the degree to which the internal variability can be accounted for by linking the rSAS function to state variables describing the hydraulic state of the reach.

3.1. Field Site Description and Hydrologic Data

The field study was conducted at the highly studied Watershed 1 (WS01) at the H.J. Andrews Experimental Forest in the Cascade Mountains, Oregon, USA (Figure 1a). The second-order stream reach has a down-valley gradient of 11.9% and valley bottom width of 10 m [*Voltz et al*., 2013]. This is a highly dissected basin, with shallow (1–2 m) and highly porous inceptisol soils underlain by bedrock. The study reach is underlain by intact bedrock, limiting the groundwater system to the valley bottom colluvium. Lateral inflows to the valley bottom from the hillslopes are expected to be minimal at the low-base flow conditions of the study [*Voltz et al*., 2013], and have also been previously represented as no-flow boundaries [*Wondzell et al*., 2009b]. On the basis of our understanding of the field site and common practices in the field, it is reasonable to neglect the role of a regional groundwater system in this location.

Field experiments focused on a highly studied stream reach of approximately 25 m located with a network of shallow subsurface wells in the stream and riparian zone [*Wondzell*, 2006]. The wells are constructed of PVC pipe screened and driven to refusal in the shallow subsurface ($\leq$1.7 m). *Wondzell et al*. [2009b] reported hydraulic conductivity ranging from 4.3×10^{-6} to 6.1×10^{-4} ms^{-1} with a geometric mean of 7.0×10^{-5} ms^{-1}. Extensive site description can be found in several related publications [*Dymess*, 1969; *Swanson and James*, 1975; *Swanson and Jones*, 2002; *Ward et al*., 2013a].

Discharge at the downstream end of the study reach was assumed equal to discharge observed at a weir that is calibrated and maintained by the U.S. Forest Service, located approximately 60 m downstream of the study reach. In past studies, gauge data were found to be representative of measured discharge values in the study reach across a wide range of discharges [*Ward et al*., 2013a]. Discharge during our study ranged

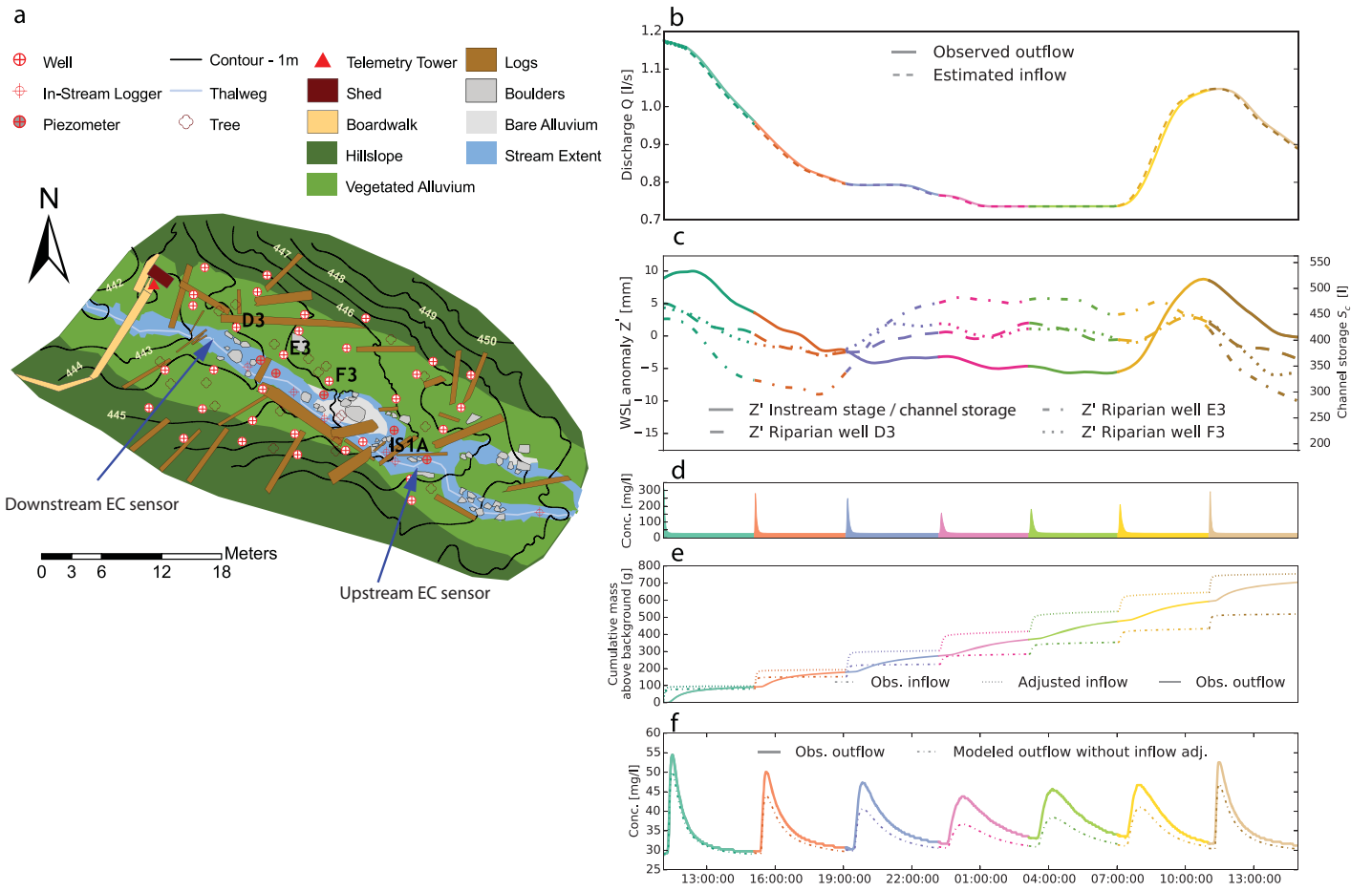

Figure 1. (a) Field study site map—modified with permission from *Voltz et al.* [2013]. Hydraulic conditions for the stream reach: (b) the U.S. Forest Service stream gauge (WS01) and (c) pressure transducers monitoring stream stage and riparian piezometers water surface level. The data have been smoothed using a Gaussian filter with a 60 min 2σ-width. The water surface level values are expressed relative to their mean during the 28 h period. The color coding is used to identify the seven 4 h periods that follow each salt tracer injection. (d) The input concentration time series, (e) the cumulative tracer mass above background, and (f) the observed and modeled (with and without inflow mass adjustment) breakthrough curves at the downstream end of the reach.

from 0.74 to 1.2 Ls^{-1}, with peak discharges occurring at approximately 12:00, and minimum discharges occurring from about 01:00 to 04:00 (Figure 1b).

Water levels in several wells and in-stream were observed using a network of pressure transducers and capacitance rods (details in *Voltz et al.* [2013]). During periods of low discharge, as in our study, diurnal fluctuations in stream discharge are common, attributed to evapotranspiration in the riparian zone and hillslopes [*Wondzell et al.*, 2009a, 2007]. *Voltz et al.* [2013] reported hydraulic gradients were down-valley dominated during the study period (i.e., down-valley gradient was steeper than cross-valley gradient), but did note observable diurnal variation in hydraulic gradients turning toward and away from the stream with changes in both stream stage and valley bottom water levels, assumed to be driven in part by hillslope discharges to the valley bottom. During our study, dynamic and heterogeneous interactions between in-stream and riparian water tables were observed (Figure 1c), demonstrating the hydrological dynamics in the system

The discharge and water level time series were smoothed using a Gaussian filter with $\sigma = 30$ min to prevent artifacts from being introduced to the analysis by the discrete jumps in measured values caused by the finite precision of the observations. The water surface elevation data in each well were normalized to have zero mean over the injection period, reported here as water surface level anomalies $Z' = Z - \bar{Z}$. A time series representing the variability of the water table gradients between the stream and riparian zone was calculated as $\Delta Z'(t) = Z'_r(t) - Z'_c(t)$, which is the difference between the water surface level anomaly averaged across the three riparian wells Z'_r, and that in the stream Z'_c. More positive values of this metric indicate stronger

gradients toward the stream, and more negative values indicate weaker gradients (though not necessarily gradients away from the stream). All time series were resampled to 1 min intervals for rSAS modeling.

3.2. Solute Tracer Injections

We conducted a series of seven in-stream slug injections of sodium chloride (NaCl) at approximately 4 h intervals. Solute tracer was mixed with stream water and injected into the stream channel one mixing length upstream of well transect H (Figure 1). Mixing lengths were visually determined [after *Day*, 1977; *Ward et al*., 2012, 2013a]. Tracer mass was nearly identical for all injections, with salt mass ranging from 100.69 to 100.87 g. In-stream specific conductivity was measured at well transect H and between well transects C and D (Figure 1) at 2 s intervals. Specific conductivity was converted to concentration using a calibration curve developed by *Ward et al*. [2012] using site water and salt tracer. Background conductivity is reported here as equivalent concentrations of NaCl. Two short periods of erroneous data were removed and filled by cubic spline interpolation. Concentration data were resampled to 1 min mean values for analysis.

3.3. Reach Water Balance Time Series

The rSAS approach requires time series of total flow into and out of the control volume in order to properly conserve the mass of water (and associated tracers). A time series of effective channel storage $S_c(t)$ and inflow $J(t)$ consistent with the observations was estimated by first fitting a simple linear regression to the stream stage data $Z'_c(t) \approx kQ(t)+Z'_0$. The effective channel storage was then assumed to be the storage above the level at which stream discharge would be zero, so $S_c(t)=(Z'_c(t)-Z'_0)BL \approx kBLQ(t)$, where B and L are the effective channel width and length, $B = 0.5$ m (approximated from visual inspection in the field at the time of the experiments) and $L = 25$ m. The effective reach inflow $J(t)$ was estimated over each 1 min interval by assuming simple kinematic wave routing $J(t)-Q(t)=dS_c/dt=kBL\,dQ(t)/dt$. This can be discretized in time and rearranged to give $J_i=Q_i+(Q_i-Q_{i-1})kBL/\Delta t$, where Q_i and Q_{i-1} are the mean outflows over adjacent periods of length Δt.

Analysis of the inflow and outflow sensor data suggested that more tracer mass apparently passed the downstream sensor during the course of the experiment than the upstream sensor. The mass that appeared to have entered upstream by the end of the experiment was considerably less than the 705 g that was introduced in the seven slugs in total. However, the outflow mass was consistent with this amount. This is likely due to incomplete mixing of the tracer across the stream at the upstream sensor. To correct for this, the inflow concentration above the background (defined as the minimum upstream concentration measured during the period, $C_{min} = 28.3$ mg/L) was adjusted using a factor f as:

$$C'_J=(f+1)(C_J-C_{\min})+C_{\min} \tag{10}$$

This factor f is an additional variable to be determined from the data. It was calibrated simultaneously with the rSAS model parameters for the "stepwise" rSAS case (described below) and the values obtained were then held constant across all other simulations.

3.4. Choice of rSAS Functional Form

Although there is a "real" well-defined rSAS function for any flux out of a control volume, it is generally only practical to observe it directly in controlled experimental conditions. Instead, a functional form for the rSAS function must be chosen and its parameters calibrated against tracer observations. Here several functional forms were examined and found to be inadequate, including a uniform distribution over a range shifted away from zero, and an exponential distribution also shifted from zero. The shifts are necessary to capture the minimum transit time for advection along the channel transport, and bring the total number of distribution parameters to two in both cases. Neither distribution was able to simultaneously capture the peak and observable tail of the tracer breakthrough curves adequately (results not shown). The three-parameter shifted gamma distribution was found to have a superior fit to the observations, and is used for all the results presented here. The cumulative form of the shifted gamma distribution can be expressed as:

$$\Omega_Q(S_T)=\frac{\gamma\left[\alpha,\frac{S_T-S_{\min}}{\beta}\right]}{\Gamma[\alpha]} \quad \text{for } S_T > S_{\min} \tag{11}$$

where $\Gamma[\alpha]$ and $\gamma[\alpha, s]$ are the gamma and incomplete gamma functions respectively [*Abramowitz and Stegun*, 1964], and α and β are referred to as the shape and scale parameters, respectively. The mean of the distribution is given by $S_\mu=\alpha\beta+S_{\min}$ and the standard deviation by $S_\sigma=\sqrt{\alpha}\beta$, both of which have units of volume.

Technically speaking, the rSAS function is only supported over the domain $[0, S]$, where $S(t)$ is the total storage in the control volume. This is inconsistent with the gamma distribution, which is defined over the domain $[0, \infty]$. However, *Harman* [2015] suggested that where the majority of the rSAS function mass is located in the younger part of the storage $S_T \ll S$ (that is, much of the storage contributes only a very small fraction of the discharge), it is reasonable to ignore this constraint. Furthermore, during a run of the rSAS model the largest value of S_T ever needed may be much less than S. In that case the shape of $\Omega(S_T)$ beyond that maximum value has no effect on the model results. This was assumed to be the case here. Longer-term tracer tests (with a tracer detectable at high dilution) would be required to determine the structure of the rSAS distribution for larger storage volumes.

3.5. rSAS Parameter Estimation and Uncertainty

The rSAS function parameters and the mass correction parameter f were estimated under different assumptions that: (1) internal variability was present, and (2) internal variability could be ignored. The model was run with the observed discharge in both cases. The model was then run with fixed discharge for both parameter sets, in order to examine the importance of external variability.

In the first case, the rSAS parameters and f were fixed within each 4 h period from one slug injection to the next, but were allowed to vary between periods. This leads to a stepwise-varying rSAS function. Parameters were fit to each period in sequence starting from the first. The model state at the beginning of the period being fit was generated using the best fit parameters for earlier periods. Thus, only three rSAS parameters (plus f) were adjusted to match each breakthrough curve. However, the parameters fitted to earlier breakthrough curves affect the fit of later ones due to the overprinting of the breakthrough curves, and the memory retained of tracer-dosed water in the age-ranked storage. Best fit parameters were estimated using an optimization routine (the Nelder-Mead simplex algorithm implemented in SciPy [*Jones et al*., 2001]) to maximize the Nash-Sutcliffe efficiency (NSE) of the predicted stream concentration relative to the observed values.

The NSE was also estimated for 240,000 rSAS parameter combinations in the vicinity of the best fit set for each period to determine the level of parameter uncertainty. The best fit stepwise-varying values of f were used in this case. For these Monte-Carlo simulations, the log-transformed parameter values were sampled uniformly from a range that bounded the best fit value.

In the second case, a set of fixed rSAS parameters was fit to the entire period by maximizing the NSE. The stepwise-varying values of f were used here also. Variations between breakthrough curves predicted using this fixed rSAS case arise only from variations in the flow rates in and out of the reach, and not from variations in transport processes within the reach.

3.6. Evaluation of Internal and External Variability

The controls of internal and external variability were evaluated using the framework described in section 2.2. A measure of the importance of each type of variability (internal and external) is the degree to which measures of model fit degrade when it is removed. Internal variability is accounted for (approximately) when the model is run with the stepwise-varying rSAS function, and eliminated when the fixed rSAS is used instead. External variability can be eliminated by running the model with a fixed time-averaged flux $Q_0 = J_0$ rather than the time-varying fluxes $Q(t)$ and $J(t)$.

The effect of removing each type of variability can be quantified by the change in the NSE, root-mean-square error (RMSE), and various summary metrics of the observed and predicted breakthrough curve shapes. For all breakthrough curve analyses, the data for the 4 h immediately following each solute tracer injection were analyzed. In addition to the observed breakthrough curve, we also analyzed the normalized breakthrough curve in an effort to minimize differences in metrics due to differences in dilution with changing discharge. Normalized concentration, $c(t)$, was calculated as:

$$c(t) = \frac{C(t)}{\int_{t=0}^{t=4hr} C(t)dt} \tag{12}$$

All analysis methods detailed here can be applied to the observed tracer time $C(t)$ series as well as the normalized time series $c(t)$. The metrics calculated using the normalized time series are denoted by the subscript "*norm*."

The first temporal moment can be calculated as:

$$M_1 = \int_{t=0}^{t=4hr} tC(t)dt \tag{13}$$

where $M_{1,norm}$ represents the mean arrival time for the tracer (conditional on it arriving within the 4 h window). Central temporal moments are calculated as:

$$\mu_n = \int_{t=0}^{t=4hr} (t - M_1)^n C(t)dt \tag{14}$$

where $\mu_{2,norm}$ represent the temporal variance of the observed tracer time series. Additionally, the coefficient of variance (*CV*, spreading normalized by advective time) and skewness (γ) can be calculated as:

$$CV = \frac{\mu_{2,norm}^{\frac{1}{2}}}{M_{1,norm}} \tag{15}$$

$$\gamma = \frac{\mu_{3,norm}}{\mu_{2,norm}^{\frac{3}{2}}} \tag{16}$$

In addition to temporal moments, several other metrics to characterize transport were calculated including the peak concentration (C_{peak}) and time of peak arrival (t_{peak}). We also calculated the holdback function (*H*) described by *Danckwerts* [1953], where $H = 0$ represents piston flow and $H = 1$ represents no movement in the system, calculated as:

$$H = \frac{1}{M_{1,norm}} \int_0^{M_{1,norm}} F(t)dt \tag{17}$$

where $F(t)$ is the cumulative distribution of the normalized breakthrough $c(t)$, calculated as:

$$F(t) = \int_{t=0}^{t} c(t)dt \tag{18}$$

The median arrival time was calculated as the value of t at which $F(t) = 0.5$.

3.7. Development of a Forward Model of Reach-Scale Transport

In addition to providing insight into the dynamics of transport in the reach, the rSAS approach provides a basis for constructing reach-scale models of solute transport. As *Harman* [2015] suggested, such a model merely requires the rSAS function (including its possible time-variability) to be specified in some way, such as by fitting functional relationships that link the parameters of an assumed distribution to some observed (or otherwise modeled) state variable(s). Here we will assume a functional relationship between the parameters of the gamma distribution and observed state variable(s) – in this case Q or $\Delta Z'$. The form of the relationship will be developed by examining how the stepwise-varying model parameters vary with these state variables, and then the model parameters will be fit to the entire breakthrough curve.

4. Results

4.1. Observed Breakthrough Curves and Variation With Discharge

Figure 1 shows the input concentration time series (Figure 1d), the cumulative tracer mass above background (Figure 1e) with and without application of the input mass correction factor *f*, and the observed breakthrough curves at the downstream end of the reach (Figure 1f). Although an identical mass of salt was used in each injection, the input concentration time series show lower peak concentrations during low flows (e.g., injection 4, pink) than high flow (e.g., injection 1, aqua) due to increased spreading of the tracer. The plot of cumulative mass of salt above background in Figure 1e clearly shows that this is not simply due to a greater attenuation of the breakthrough curve at low flows. Nor is it due to a change in the background concentration. During the injection period, the background solute concentration was quite stable. Ninety percent of the electrical conductivity values measured at the upstream sensor were equivalent to values

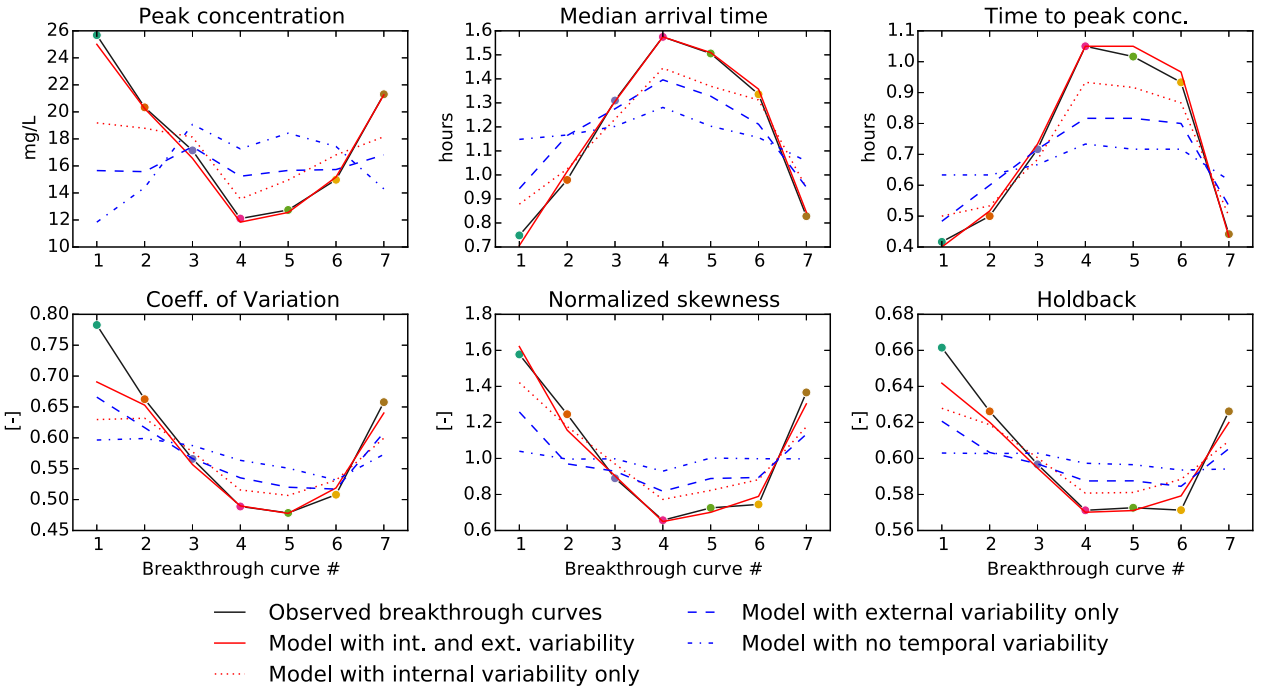

Figure 2. Comparison of breakthrough curve summary metrics for the observed breakthrough, and for the four modeled cases.

between 28.3 and 32.0 mg/L of NaCl (though the actual stream solute composition is not known)—close to the initial concentration at the downstream of 28.8 mg/L.

The best fit values of f vary across the experiment from low values at the start and end (21% and 28% for injections 1 and 7) to high values in the middle (91% during injection 4). Figure 1 illustrates the importance of the mass adjustment factor f. The dash-dot line in the lower plot (Figure 1f) show the best fit model output (described below) when $f = 0$, representing no adjustment of the input concentration. The predicted concentrations are consistently lower than the observed.

The shape of the seven breakthrough curves varied considerably over the course of the experiment (Figure 1f). Breakthrough curves during lower discharge conditions were generally characterized by lower peak concentrations, later mean arrival times, later time to peak concentration, decreased coefficient of variation (spreading relative to travel time), decreased skewness, and decreased holdback (Figure 2). Note that these breakthrough curve metrics are affected by the finite duration of the breakthrough curve observation (4 h) and the overprinting of the tail of each breakthrough curve by the breakthrough of the subsequent injections (i.e., the stream did not return to the background level).

4.2. Structure of the Fitted rSAS Functions

The stepwise-varying rSAS function is able to produce predictions almost identical to the observations (Figure 3). Table 1 gives the four parameter values fit to each slug, along with the calculated values of S_σ and β, and the root-mean-square error (RMSE) and Nash-Sutcliffe model efficiency (NSE) for each of the seven injection periods. The best fit RMSE was between 0.13 and 0.37 mg/L and the NSE is more than 0.995 for all seven periods (a NSE of 1 represents a perfect fit). The shape of the stepwise-varying rSAS function is illustrated in Figure 3.

The uncertainty in the shape parameter α and scale parameter β are both considerably greater than the uncertainty in the mean and standard deviation S_μ and $S\sigma$, which are tightly constrained by the breakthrough curve data. The mean of the fitted rSAS function begins at $S_\mu = 3.0$ m^3 during the first period, rises to a maximum of 5.0 m^3 in the fourth period, and then declines. The standard deviation S_σ rises quickly over the first few periods, peaks in event three, and then slowly declines. These variations produce a distinct elongation and shift in the mode of the rSAS function toward larger S_T, implying that the outflow contains a larger fraction of older water during periods 4, 5, and 6, when flow is lowest. Variations in S_{min} values from

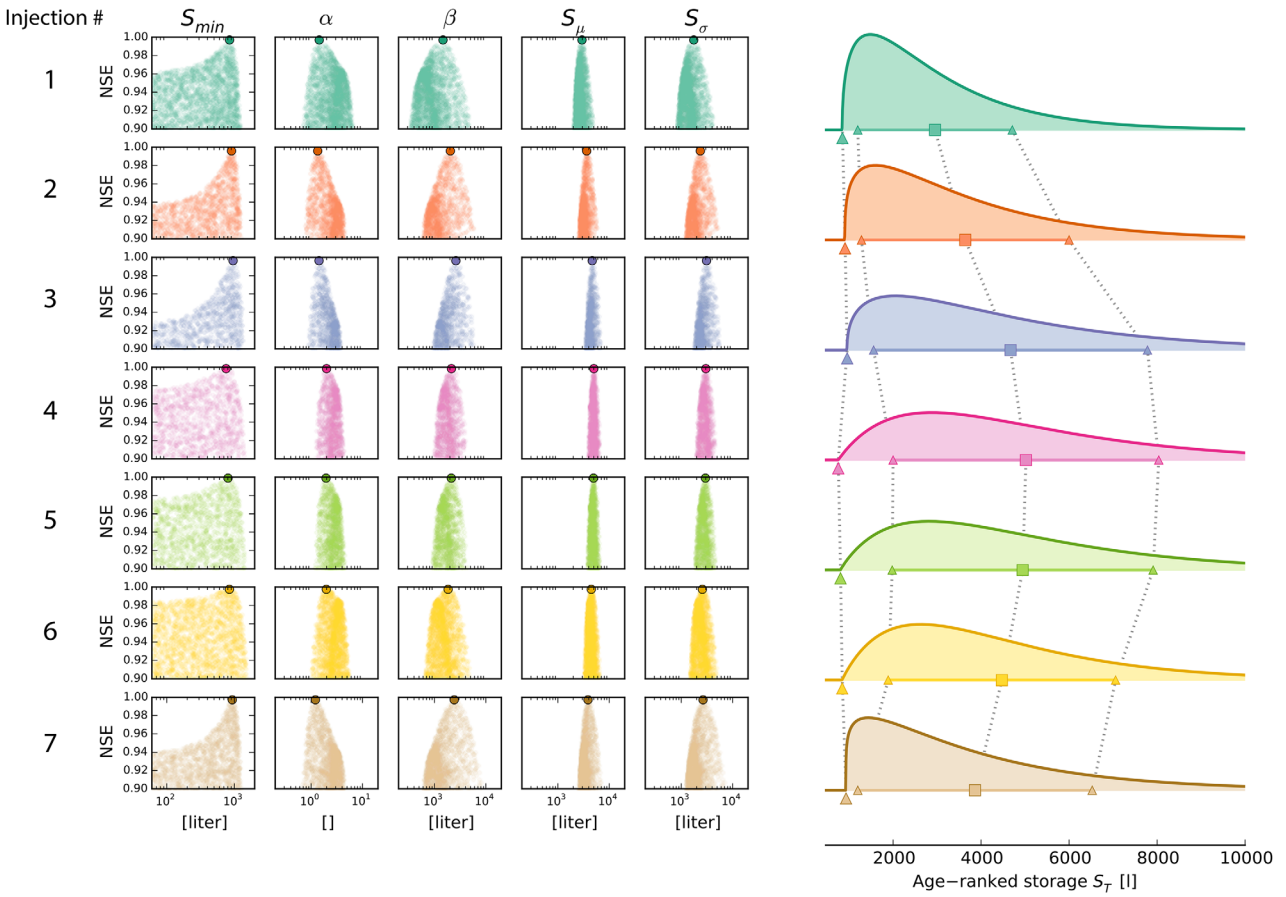

Figure 3. Parameter estimation for the gamma distribution rSAS function fit to reproduce the breakthrough curve of each breakthrough curve. Dotty plots on the left show the Nash Sutcliffe Efficiency (NSE) of the Monte-Carlo parameter estimates. The rSAS functions given by the best fit parameters are shown on the right. The distribution can be specified by the offset S_{min} (given by the triangle), the mean (square), and the standard deviation (indicated by left-pointing and right-pointing triangles).

slug to slug were smaller, and the uncertainties were larger, so it is not immediately clear whether this parameter shifts significantly in time.

4.3. Internal and External Transit Time Variability, and Effects on Breakthrough Curves

The importance of internal and external variability is illustrated in Figure 4. The results are shown for models where both types of variability are accounted for, and with external variability only, internal variability only, and with neither type of variability. Note that when internal variability is removed (Figure 4, second and fourth rows), the rSAS function is invariant in time, by definition. The presence of external variability (Figure

Table 1. Value of the rSAS Distribution Parameters for the Best Fit Stepwise rSAS Model, Where the Parameters are Allowed to Vary in a Stepwise Way at the Moment Each of the Seven Tracer Injections Occurred, Along With the Root-Mean-Square Error (RMSE) and Nash-Sutcliffe Efficiency (NSE) Calculated for Each Period[a]

	α	β (L)	S_{min} (L)	S_μ (L)	S_σ (L)	f (%)	RMSE (mg/L)	NSE
Slug 1	1.44 (−10/43%)	1465 (−34/21%)	849 (−22/7%)	2953 (−11/7%)	1756 (−21/14%)	19	0.35	0.9971
Slug 2	1.34 (−10/20%)	2036 (−20/15%)	908 (−13/10%)	3641 (−6/5%)	2359 (−12/9%)	36	0.36	0.9959
Slug 3	1.42 (−6/8%)	2609 (−9/10%)	957 (−12/4%)	4669 (−3/3%)	3112 (−7/7%)	53	0.30	0.9963
Slug 4	2.00 (−14/24%)	2137 (−20/21%)	754 (−35/21%)	5019 (−7/7%)	3019 (−12/12%)	91	0.14	0.9985
Slug 5	1.95 (−15/28%)	2123 (−21/17%)	806 (−43/23%)	4945 (−6/5%)	2964 (−11/10%)	68	0.13	0.9990
Slug 6	1.97 (−18/38%)	1840 (−28/28%)	845 (−48/25%)	4473 (−9/9%)	2584 (−17/17%)	40	0.23	0.9977
Slug 7	1.21 (−12/17%)	2421 (−16/27%)	931 (−12/9%)	3862 (−7/11%)	2664 (−11/19%)	27	0.31	0.9973
Fixed	1.51	2296	870	4333	2820		1.69	0.9179

[a]Parameters with units are given in liters. The overall RMSE was 0.29 mg/L and NSE was 0.9976. Uncertainty in each parameter is given by the range of values for which the NSE > 0.99, expressed as percentage change (±%) from the best fit value.

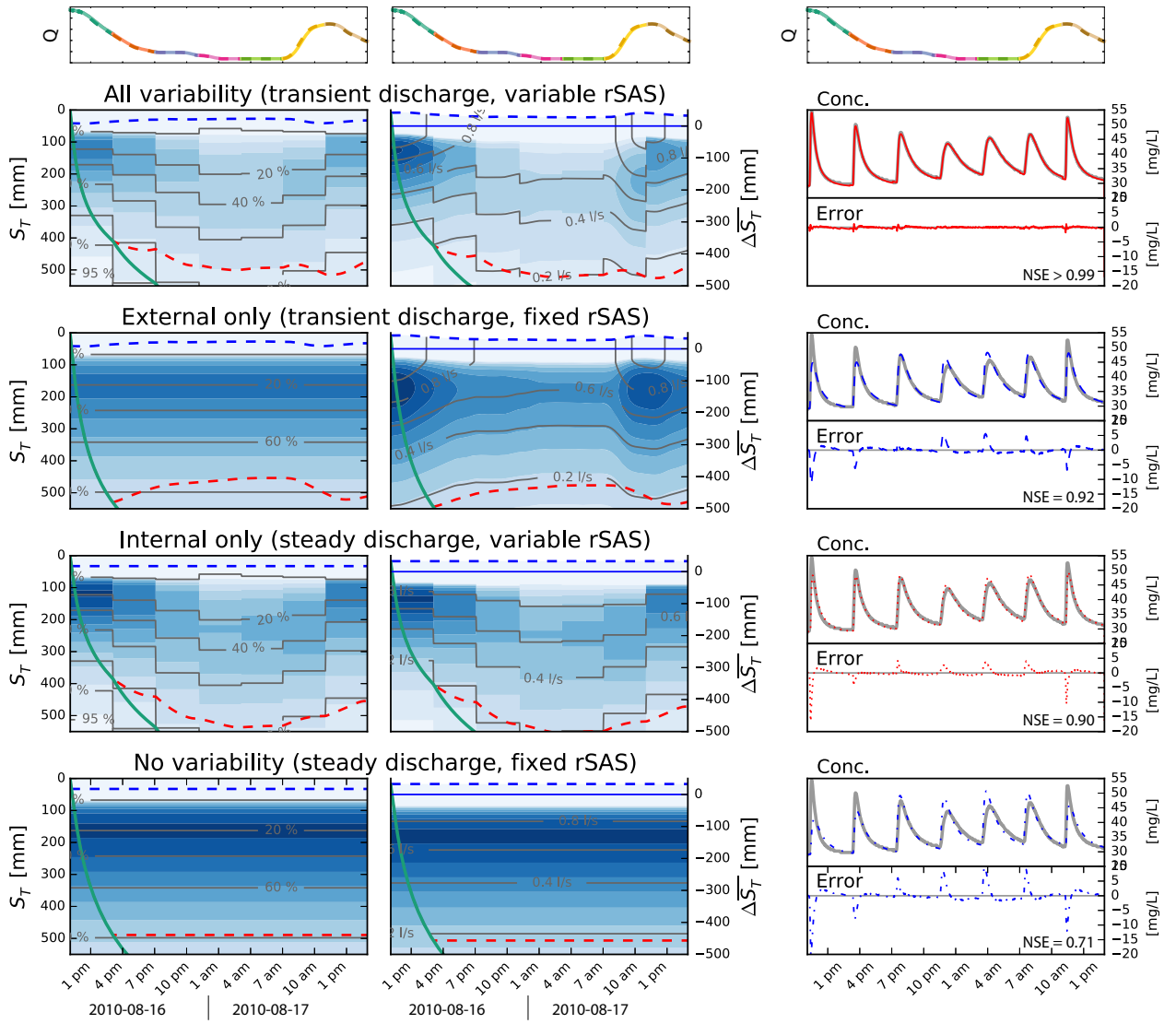

Figure 4. Plots showing (left, center) the structure of the rSAS function and (right) the predicted (colored) and observed (gray) breakthrough curves, along with their residual error. The results are given for the best fit piecewise-varying rSAS function (top) for the case with only external and only internal variability and (bottom) for the case with no transport variability. Discharge is shown at the top of each column for reference. The left and center plots illustrate the structure of the storage selection in two different ways. Plots on the left show the rSAS function as a density $\omega(S_T, t)$ (in the blue shaded contours) and as a cumulative distribution $\Omega(S_T, t)$ (in the grey contours). Each of the rSAS functions in Figure 3 is equivalent to a vertical slice through the top-left subplot in this figure. The center plots show the unnormalized complementary rSAS function in cumulative ($\overline{Q_T}$) and density ($\partial\overline{Q_T}/\partial\Delta\overline{S_T}$) forms (equations (8) and (9), respectively). The area above the green line is the portion of storage younger than the first tracer injection, and the area above the red dashed line is younger than 4 h. Storage values in these plots have been normalized by the channel surface area (nominally 25 m $\times$ 0.5 m) and converted to millimeters.

4, second row) means that more discharge is removed from some age-ranks in storage at high flows than low flows, but the proportion of discharge from those parts of the storage is invariant. When external variability is absent (Figure 4, third and fourth rows), the rSAS and complementary rSAS functions are identical up to a scalar multiple (discharge) and constant offset (relative storage).

The plots of the complementary rSAS function for best fit case (Figure 4, top row, center plot) show an interesting behavior. Below about -200 mm of age-ranked storage (equal to about -2500 L of storage in the reach), the rate of discharge is more or less constant at around 0.6 L s^{-1}. This suggests that during the higher flow periods (at the start and end of the observed period), the variations in discharge are primarily accommodated by more rapidly turning over the younger storage. The slower flow pathways are relatively unperturbed by an increase in streamflow. In fact, the results suggest that the rate of discharge from the older storages declines when overall flow rate increases.

The observed breakthrough curves are best reproduced when both internal and external variability are accounted for. When internal variability is removed (the fixed rSAS case) RMSE increases to 1.69 mg/L and NSE declines to 0.9. When external variability is removed (variable rSAS but constant flux Q_0) RMSE = 1.64 mg/L and NSE = 0.91. When both are removed (fixed rSAS and constant flux Q_0) RMSE = 2.9 mg/L and NSE = 0.71.

The effects are further illustrated by the metrics of breakthrough curve shape (Figure 2). The model runs with both internal and external variability generally match the observed metrics very well. These both tend to show a large U-shaped variation in breakthrough curve properties over the course of the seven injections.

Removal of internal and/or external variability tends to flatten, if not completely reversed, this pattern of variation. For example, the observed time to peak concentration varies from 0.4 to 1.1 h, but when internal or external variability is removed the arrival times become less varied. When both are removed, the modeled time to peak becomes almost invariant. Similar patterns can be seen for the median arrival time, coefficient of variation, skewness and holdback. The peak concentration goes further: when the variability is removed the peak concentration is highest, rather than lowest, for the middle set of events.

4.4. Correlation of rSAS Internal Variability With Discharge and Riparian Potential Gradients

Relationships with Q and $\Delta Z'$ are strongest for the central moments of the rSAS distribution, and weaker for the parameters (Figure 5). The mean S_μ increases systematically with $\Delta Z'$, and decreases with Q. The standard deviation S_σ decreases with Q and shows some tendency to increase with $\Delta Z'$, but the relationship is not as strong. In contrast, the scale parameter β does not appear to vary systematically with either Q or $\Delta Z'$. The high values of the shape parameter α in periods 4, 5, and 6 are associated with low (or increasing) Q and high (or decreasing) $\Delta Z'$. The low values in the other events are associated with a range of Q, but seem to be clustered around low (or increasing) values of $\Delta Z'$. Variations in S_{min} parameter are weak and generally smaller than the range of values in the $NSE > 0.99$ bounds. The f parameter (Table 1) shows clearer relationships, decreasing with Q and increasing with $\Delta Z'$.

The relationships shown in Figure 5 suggest that both state variables are typically better correlated with the moments of the distribution than with the parameters per se, and the correlations appear to be linear. Thus, to construct a forward model, we might assume functional relationships of the form:

$$S_\mu = a_\mu X + b_\mu \tag{19}$$

$$S_\sigma = a_\sigma X + b_\sigma \tag{20}$$

$$S_{\min} = a_{\min} X + b_{\min} \tag{21}$$

where X is either ΔQ (the variation in discharge around the mean, $Q - \bar{Q}$) or $\Delta Z'$. Values of the a and b parameters were calibrated by minimizing the RMSE error with the observed breakthrough curve concentrations. The resulting models relating rSAS parameters to Q or $\Delta Z'$ are also plotted in Figure 5, along with the fixed rSAS parameters for comparison, and the best fit model parameters are given in Table 2.

Results demonstrate that models based on Q and $\Delta Z'$ perform similarly (which is unsurprising given their covariation) at a level somewhat below that of the piecewise-varying rSAS (Nash-Sutcliffe efficiency of 0.97–0.98 rather than >0.99) but considerably better than the fixed rSAS (0.92). The effects on the predicted rSAS function and breakthrough curve predictions are given in Figure 6. Both models are able to reproduce the major features of the rSAS function and match the breakthrough curves well. Much of the error seems to be associated with the timing of the initial breakthrough. This was expected, since the timing is controlled by S_{min}, and this parameter had relatively little relationship to the observed state variables.

5. Discussion

5.1. rSAS as a Process-Agnostic Interpretation Framework

As demonstrated above, reach-scale transport dynamics can be reproduced by the rSAS model. This supports the use of rSAS as a method for analyzing and interpreting stream solute tracer studies in a "process-agnostic" way. We describe the rSAS framework as process-agnostic in the sense that the key outcome is the rank Storage Selection function, which is not based on a suite of conceptual storages and fluxes and

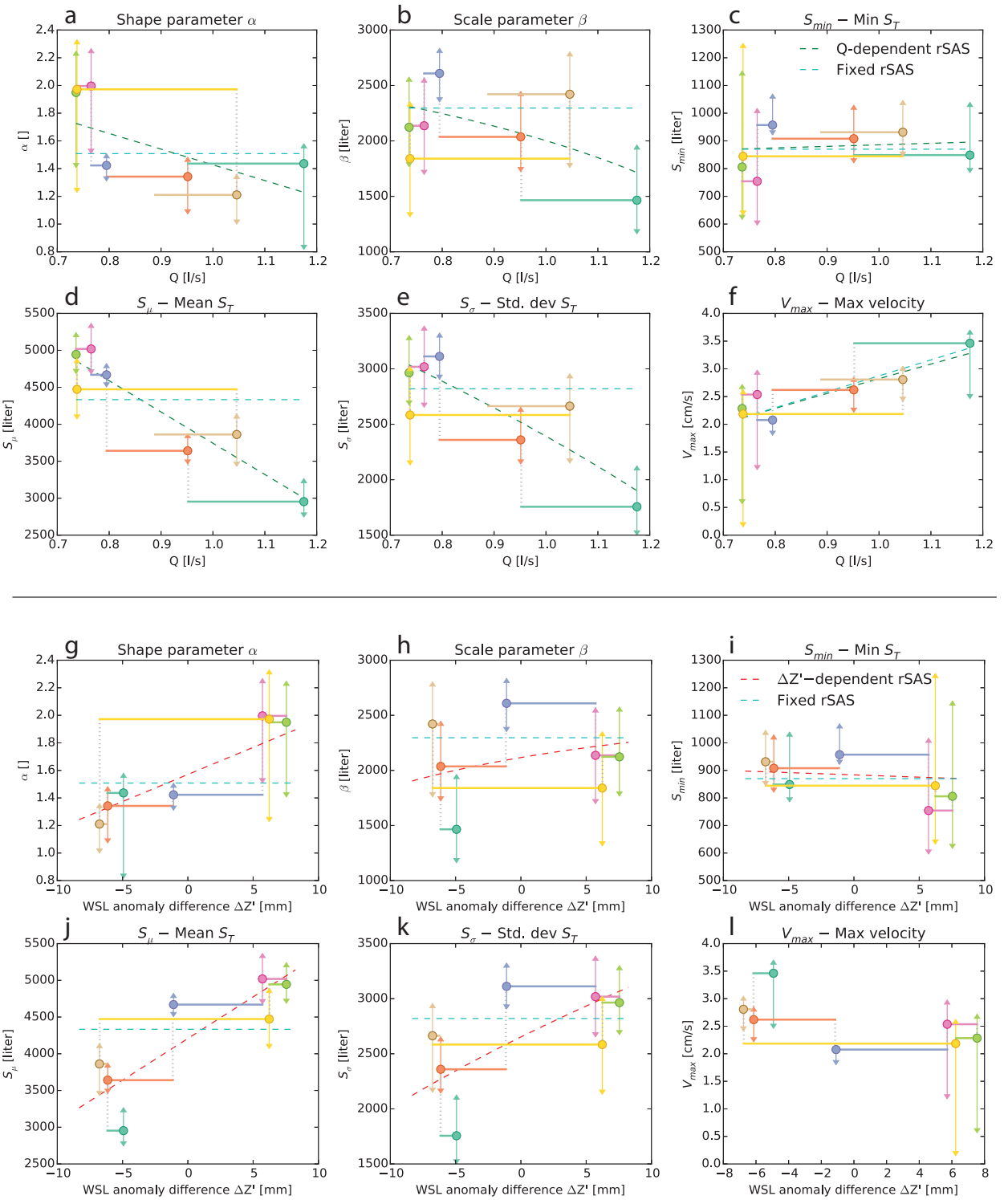

Figure 5. Parameters of the rSAS function plotted against (a–f) discharge and (g–l) $\Delta Z'$. Circles indicate the discharge at the time of the tracer injection, and the associated horizontal lines indicate the variation in Q over the subsequent 4 h. Error bars indicate the range of parameters that provide model fits with NSE $>$ 0.99. Vertical dotted lines link adjacent periods. The fixed and $Q/\Delta Z'$ models are shown in the dashed lines. More positive values of $\Delta Z'$ indicate larger water potential gradients toward the stream.

their effective parameters. This makes the rSAS approach different in three key ways, as compared to other approaches where model parameters arise from explicit separation of transport processes into conceptual domains.

Table 2. Alternative Models of the rSAS Model Parameters and Their Associated Performances[a]

Model	Parameter Submodels	RMSE (mg/L)	NSE
Discharge	S_μ (L) = −4084.62 ($Q-\bar{Q}$) + 4279.39	0.75	0.9739
	S_σ(L) = −2431.81 ($Q-\bar{Q}$) + 2698.59		
	S_{min}(L) = 59.51 ($Q-\bar{Q}$) + 873.64		
Riparian	S_μ(L) = 112.54 $\Delta Z'$ + 4197.71	0.66	0.9771
	S_σ(L) = 58.37 $\Delta Z'$ + 2628.58		
	S_{min}(L) = −1.78 $\Delta Z'$ + 876.47		

[a]Q in liter per second, $\Delta Z'$ in millimeter, f in percentage, and S_{min} and S_μ in liter. Mean discharge is $\bar{Q}$ = 0.870 L/s.

First, the rSAS approach treats the stream-hyporheic system as a continuum rather than as distinct domains with different process representations. In contrast, common frameworks such as the transient storage model [*Bencala and Walters*, 1983], Advection Storage-Path model [*Worman et al.*, 2002], and STAMMT-L [*Haggerty et al.*, 2000] assign specific advective, dispersive, and storage processes to distinct domains. In these models, streams are represented as a one-dimensional domain with advection and longitudinal dispersion. Transient storage may be represented as an additional single domain or multiple domains [*Kerr et al.*, 2013; *Briggs et al.*, 2009; *Choi et al.*, 2000], each of which is characterized by some specified transit time distribution. There is considerable overlap in the time scales of retention in in-stream transient storage and in rapid hyporheic exchange. Thus, (1) both can simultaneously act on breakthrough curves, (2) their effects cannot be distinguished based on in-stream observations alone [*Kelleher et al.*, 2013], and (3) model storage domains cannot be explicitly said to be surface or subsurface storage domains. The rSAS approach represents the system as a continuum of age-ranked storage, varying from the advection-dominated stream (the most mobile water, and most preferentially sampled in our results; the top of Figure 4) to the water that is functionally immobile during the experiment (the least mobile water, minimally sampled in our study; the bottom of Figure 4).

Second, the rSAS framework accounts for the effect of internal variability on transit time distributions throughout the system. Transport processes such as dispersion and groundwater discharge into streams are expected to vary with discharge. The existing models outlined above have primarily been applied during steady flow conditions where the parameters describing processes are fixed in time. One notable exception is the unsteady state flow routing coupled to the transient storage model implemented by *Runkel et al.* [1998], where stream area and discharge were allowed to vary in time, but all other transport parameters (representing dispersion and transient storage) were fixed. The ability to continuously vary all parameters with discharge could be implemented in those existing models where conceptual compartments are

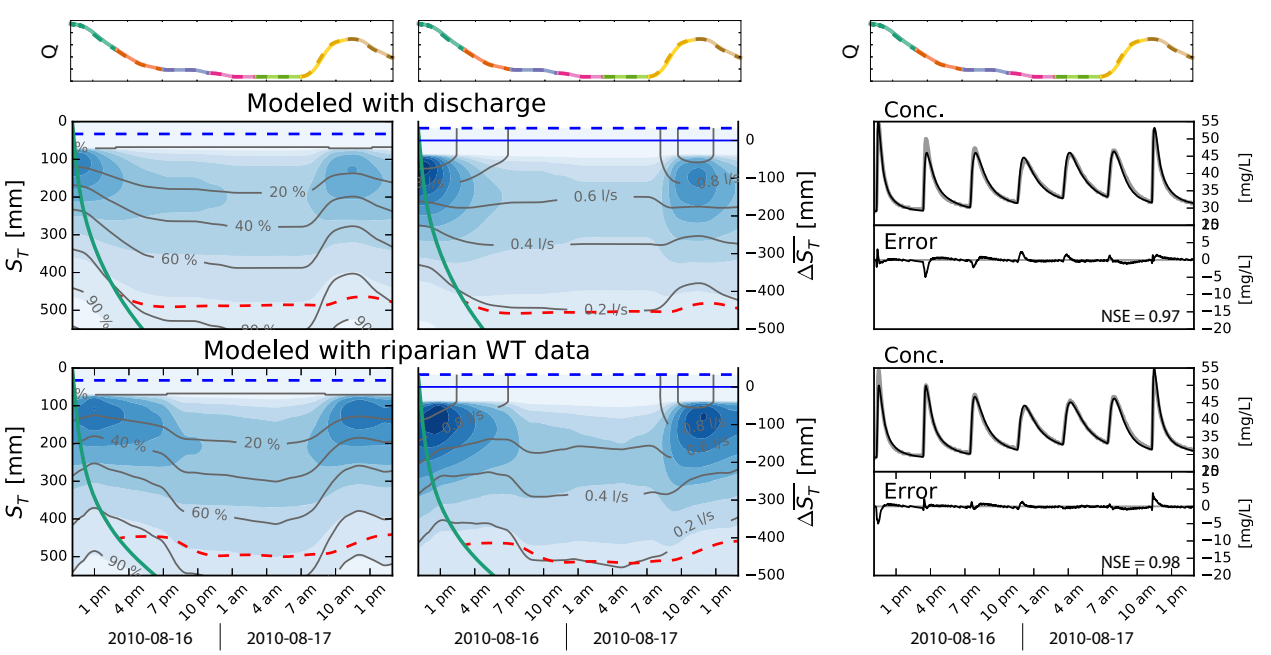

Figure 6. Similar plots to Figure 4 but with rSAS functions predicted from (top) the discharge and (bottom) the riparian water table elevation. Discharge is shown at the top of each column for reference.

assumed to be well mixed, but these steps have not been implemented in the commonly used models, some of which have been in use for more than 30 years. Models that assume fixed transit time distributions for transient storage cannot be modified to have time-varying parameters without violating mass balance.

Third, the time-variability of transport is decomposed into internal and external variability, whose effects can then be quantitatively compared. As Figures 2 and 4 demonstrate, these two types of variability both contribute significantly to the changing structure of the breakthrough curve in this case. Thus, the two hypotheses articulated in the introduction are both rejected—neither internal nor external variability dominate the time-variability of the stream-hyporheic transport.

5.2. Internal Variations in Reach-Scale Transport

We can examine the shape of the rSAS function and its variations between the seven injections, and speculate on the underlying physical process dynamics. This study site has been well characterized in past research, so there is an established body of understanding to anchor this speculation. However, the nearly 12 h phase shift in diel fluctuations in the stream at this discharge (documented by *Wondzell et al*. [2007]) complicates interpretation, making it difficult to determine whether a change in the shape of the rSAS function is associated with changing discharge or changing near-stream potential fields.

It was unexpected that variations in the S_{min} parameter would be so apparently uncorrelated with discharge. This parameter represents the volume of water that has entered the system in the time it takes for a water parcel taking the fastest transport pathway to travel the length of the reach. It might be called the "minimum advective displacement volume." We had initially expected S_{min} to scale proportionally with channel storage. The channel storage and S_{min} did tend to vary over a similar range (around 200 L), but they varied so little compared to the uncertainty in S_{min} that a correlation between them could not be distinguished. In general, S_{min} was around twice as large as the apparent channel storage.

The near invariance of S_{min} does not contradict observations of discharge-dependent variations in channel velocity and advective breakthrough time. At a given discharge and S_{min}, the time taken for the initial breakthrough would be $T_{\min}=S_{\min}/Q$, and so the maximum velocity (assuming constant discharge) along a reach of length $\ell = 25$ m would be $v_{\max}=Q\ell/S_{\min}$. This maximum velocity is plotted as a function of discharge in Figure 5, and shows a clear positive relationship, as would be expected.

Admittedly, the observed variation in discharge during the study was small, and it is likely that the value of S_{min} would be different at higher flows. However, it is not clear what the form of this variation would be. It may be that at higher flows, the larger volume of the main channel flow would lead to a proportional increase in S_{min}. Conversely, this may be counteracted by the concurrent increase in dispersion, such that the first breakthrough of tracer traveling along the fastest pathway through the reach arrives after a relatively small volume of water has entered the reach.

Since S_{min} hardly changes, the changes in the mean of the rSAS function over time are primarily due to changes in the shape of the gamma distribution. Changes in the mean S_μ and standard deviation S_σ are correlated with both the riparian water table variations $\Delta Z'$ and the discharge Q (Figure 5). The results suggest that S_μ and S_σ tend to be smallest when discharge (and consequently channel storage) is highest, and when the riparian water table is lowest. Thus, for low Q and a high $\Delta Z'$, discharge is dominated by older water drawn from a wide range of ages, whereas for high Q and low $\Delta Z'$ the age distributions are dominated by younger water.

These shifts in the parameters of the rSAS function suggest that the diel variations in base flow discharge are accommodated by variations in the turnover rate of the youngest part of the reach storage. However, the volume of this dynamic part of the storage is considerably larger than the apparent volume of the channel. As Figure 4 shows, this volume is approximately equal to the volume of the channel plus 2500 L (or more specifically, $\Delta\overline{S_T}=-200$ mm, when normalized by channel area, Figure 4, top row). In other words, the dynamic part of the storage is approximately 4 times larger than the channel volume (which is typically less than 50 mm deep). The volume that is turning over more slowly is substantial, and its turnover rate is relatively steady. The volume older than the "channel-plus-2500 L" consistently contributes about 0.6 L/s to the discharge. This represents 80% of the discharge at the lowest flow. Approximately 0.2 L/s is consistently delivered by water that is older than 4 h (red dashed line in Figure 4).

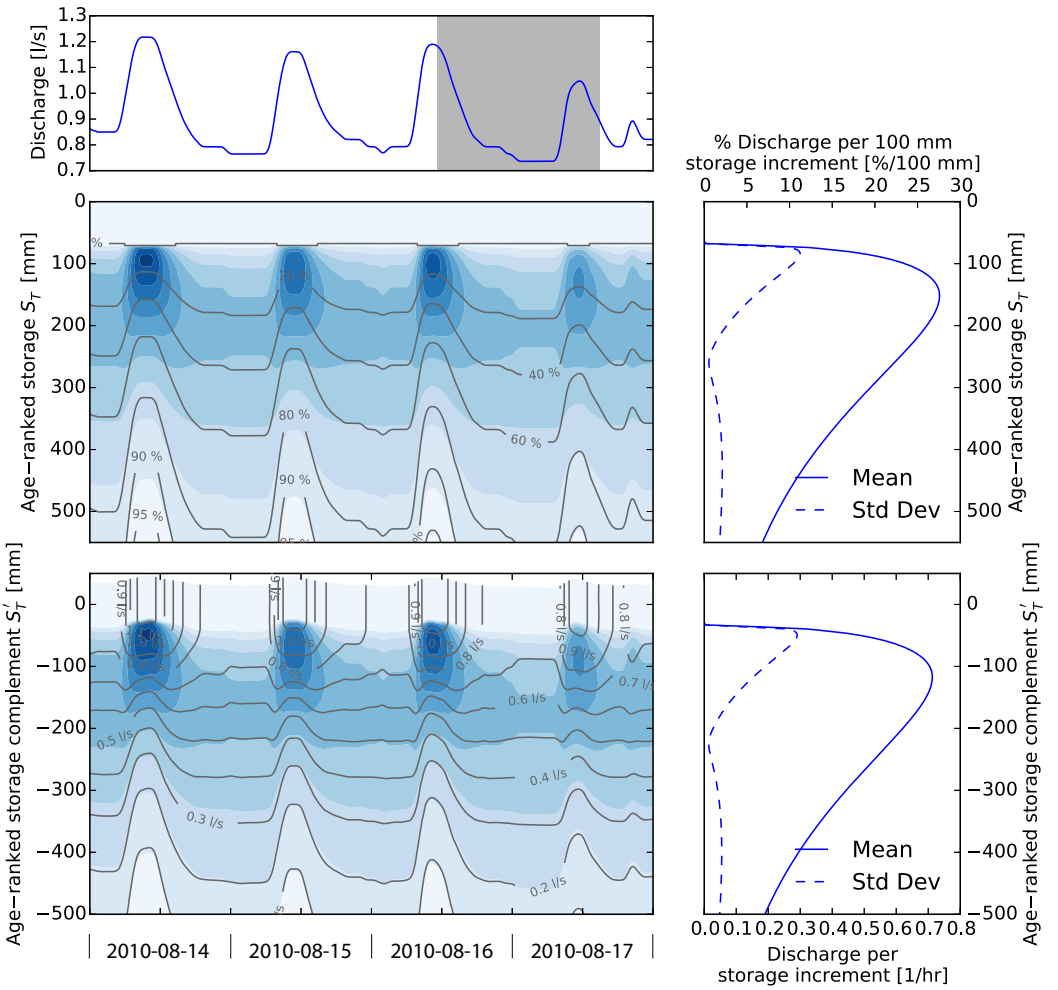

Figure 7. Structure of the rSAS function predicted from observed discharge over a 4 day period up to and including the study period. Study period is highlighted in grey in the top figure. Contour plots show (top) the rSAS function $\Omega(S_T, t)$ and (bottom) the $\overline{Q_T}(\Delta\overline{S_T}, t)$ function. Plots on the right show the mean and standard deviation of the density forms of the functions at each value of S_T and $\Delta\overline{S_T}$.

The extent to which the variations in the riparian water table contribute to this pattern is not clear. Previous studies have suggested that high riparian water tables could be associated with a contraction of the hyporheic zone [*Cardenas and Wilson*, 2007; *Cardenas*, 2009; *Storey et al.*, 2003]. Here in contrast, the apparent volume turning over most quickly is largest in the middle of the experiment, when the riparian water tables are highest. Furthermore, as Figure 4 shows, the apparent turnover rate in the older part of the storage may be higher during the high-water table period (indicated by the downward deflection of the 0.2 L/s contour in the top center figure). This is inconsistent with an immobilization of older water when the riparian water table is high. This observation is close to the edge of the window of detection of the experiment (i.e., the 4 h aged water indicated by the red dashed line in Figure 4), and so this result cannot be considered conclusive. It may in fact be an artifact of the gamma-distribution functional form—the increased relative discharge above $\Delta\overline{S_T} = -200$ mm requires the function to "pivot," reducing the amount of discharge below $\Delta\overline{S_T} = -200$ mm. More sophisticated functional forms for the rSAS function must be explored to examine this possibility.

5.3. Toward a Time-Variable rSAS Parameterization at the Reach Scale

The results also indicated the feasibility of using rSAS as a basis for forward modeling of reach-scale transport. As an illustration of how this type of model can be used, the discharge-dependent model was applied to the 4 days up to and including the study period. Discharge over that period varies over a consistent range, so the results do not require extrapolation of the model relationships. The results are shown in Figure 7. The top and bottom contour plots correspond to the left and right plots in Figures 4 and 6. The plots on the right summarize how discharge is extracted from storage over the modeled periods. These distributions

show that the pattern identified for the experimental period is repeated in time. Most of the time-variable discharge is drawn from the youngest $\Delta\overline{S_T} > -200$ part of the storage, and discharge from $\Delta\overline{S_T} < -200$ is relatively steady, apart from a reduction during the high flows (which may be artifactual).

To extend this kind of modeling approach to other hydraulic conditions and other reaches where tracer data are not available, we must understand the relationship between the rSAS function and the physical structure of stream reaches. There is good reason to hope that such a mapping from landscape to model is possible, since the rSAS function is a distribution over the real storage volume of water within the reach. Thus investigation of the rSAS function can proceed by identifying how age-ranked storage is distributed in space, and how the transport processes operating within the reach determine the shape of the rSAS function. For example, a more accurate survey of in-channel volume would help determine the extent to which in-channel transient storage (for instance, in pools and eddies unrepresented by the crude channel volume estimate used here) is sufficient to fully account for the 200 mm of dynamic turnover storage. Subsurface observations of storage and/or transport could also be used to determine the volume in the bed that is turning over on those time scales, and thus map the age-rank storage back into the landscape.

6. Conclusions and Future Research

This application of the rank Storage Selection (rSAS) theory to a sequence of tracer breakthrough curves in a small stream has demonstrated the ability of this approach to reproduce the observed transport dynamics, to provide insight into the time-varying turnover of storage volumes within the reach, and to examine the covariation of that internal variability with the controlling state variables.

Rather than support one of the "contradictory" hypotheses established in the introduction to this paper, the results suggest that both internal and external variability control the temporal variability of transit times through the reach. The diel increases in discharge are accommodated in the reach by an increase in the turnover rate of a volume of water approximately 4 times larger than the channel. In addition, a large portion of the discharge is supplied by turnover of older water, and the rate of that turnover is relatively unperturbed by the variations in discharge. This likely represents Darcian flow through the hyporheic zone driven by the (relatively unchanging) topographic gradient of the valley bottom. Variations in the turnover of these slower flow paths are unlikely to be driven by variations in riparian water tables, and may be artifacts.

We have also shown that this approach can be used to construct a model of the time-varying rSAS function in terms of the observed state variables of discharge and riparian water table elevations. These models were able to similarly reproduce the transport dynamics. As such, we believe this approach holds promise as a basis for constructing reach-scale transport models that can act as elements of a time-variable solute transport models at the network scale.

Acknowledgments

Thanks to Celine Cua for contributions to data analysis. C. J. *Harman* acknowledges the support of NSF grants NSF EAR-1344664 and CBET-1360415. Ward was supported by the NSF grant EAR-0911435. Tools for solute tracer time series analyses were developed by Ward and others with support provided in part by the NSF grant EAR 1331906 for the Critical Zone Observatory for Intensively Managed Landscapes (IML-CZO), a multi-institutional collaborative effort. Ward was also supported by the Indiana University Office of the Vice Provost for Research. Data and facilities were provided by the H.J. Andrews Experimental Forest research program, funded by the NSFs Long-Term Ecological Research Program (DEB-1440409), US Forest Service Pacific Northwest Research Station, and Oregon State University. Any opinions, findings, and conclusions or recommendations expressed in this material are those of the authors and do not necessarily reflect the views of the National Science Foundation, U.S. Forest Service, H.J. Andrews Experimental Forest, Oregon State University, or Indiana University. Discharge data are available from the H.J. Andrews Experimental Forest Data Catalog (http://andrewsforest.oregonstate.edu/). In-stream specific conductance time series are available upon request to Ward (adamward@indiana.edu). The authors declare no conflicts of interest.

References

Abramowitz, M., and I. A. Stegun (1964), *Handbook of Mathematical Functions: With Formulas, Graphs, and Mathematical Tables*, vol. 55, Dover Publications Inc., N. Y.

Bencala, K. E., and R. A. Walters (1983), Simulation of solute transport in a mountain pool-and-riffle stream: A transient storage model, *Water Resour. Res.*, *19*(3), 718–724, doi:10.1029/WR019i003p00718.

Bencala, K. E., M. N. Gooseff, and B. A. Kimball (2011), Rethinking hyporheic flow and transient storage to advance understanding of stream-catchment connections, *Water Resour. Res.*, *47*, W00H03, doi:10.1029/2010WR010066.

Botter, G., E. Bertuzzo, and A. Rinaldo (2010), Transport in the hydrologic response: Travel time distributions, soil moisture dynamics, and the old water paradox, *Water Resour. Res.*, *46*, W03514, doi:10.1029/2009WR008371.

Briggs, M. A., M. N. Gooseff, C. D. Arp, and M. A. Baker (2009), A method for estimating surface transient storage parameters for streams with concurrent hyporheic storage, *Water Resour. Res.*, *45*, W00D27, doi:10.1029/2008WR006959.

Cardenas, M. B. (2009), Stream-aquifer interactions and hyporheic exchange in gaining and losing sinuous streams, *Water Resour. Res.*, *45*, W06429, doi:10.1029/2008WR007651.

Cardenas, M. B., and J. L. Wilson (2007), Exchange across a sediment-water interface with ambient groundwater discharge, *J. Hydrol.*, *346*(3-4), 69–80, doi:10.1016/j.jhydrol.2007.08.019.

Choi, J., J. W. Harvey, and M. H. Conklin (2000), Characterizing multiple timescales of stream and storage zone interaction that affect solute fate and transport in streams, *Water Resour. Res.*, *36*(6), 1511–1518.

Danckwerts, P. V. (1953), Continuous flow systems: Distribution of residence times, *Chem. Eng. Sci.*, *2*(1), 1–13.

Day, T. J. (1977), Field procedures and evaluation of a slug dilution gauging method in mountain streams, *J. Hydrol. N. Z.*, *16*(2), 113–133.

Dudley-Southern, M., and A. Binley (2015), Temporal responses of groundwater-surface water exchange to successive storm events, *Water Resour. Res.*, *51*, 1112–1126, doi:10.1002/2014WR016623.

Dymess, C. T. (1969), Hydrologic properties of soils on three small watersheds in the western Cascades of Oregon, *USDA For. Ser. Res. Note PNW-111*, 17 pp., Pacific Northwest Forest and Range Experiment Station, Portland, Oreg.

Fischer, H. B., J. E. List, C. R. Koh, J. Imberger, and N. H. Brooks (1979), *Mixing in Inland and Coastal Waters*, Academic, San Diego, Calif.
Gooseff, M. N., K. E. Bencala, and S. M. Wondzell (2008), Solute transport along stream and river networks, in *River Confluences, Tributaries, and the Fluvial Network*, edited by S. P. Rice, A. G. Roy, and B. L. Rhoads, pp. 395–418, John Wiley, Hoboken, N. J.
Haggerty, R., S. A. McKenna, and L. C. Meigs (2000), On the late-time behavior of tracer test breakthrough curves, *Water Resour. Res.*, *36*(12), 3467–3479, doi:10.1029/2000WR900214.
Harman, C. J. (2015), Time-variable transit time distributions and transport: Theory and application to storage-dependent transport of chloride in a watershed, *Water Resour. Res.*, *51*, 1–30, doi:10.1002/2014WR015707.
Harvey, J. W., and K. E. Bencala (1993), The Effect of streambed topography on surface-subsurface water exchange in mountain catchments, *Water Resour. Res.*, *29*(1), 89–98.
Harvey, J. W., B. J. Wagner, and K. E. Bencala (1996), Evaluating the reliability of the stream tracer approach to characterize stream-subsurface water exchange, *Water Resour. Res.*, *32*(8), 2441–2451, doi:10.1029/96WR01268.
Jones, E., T. Oliphant, and P. Peterson (2001), SciPy: Open source scientific tools for Python. [Available at http://www.scipy.org/.]
Kelleher, C., T. Wagener, B. McGlynn, A. S. Ward, M. N. Gooseff, and R. A. Payn (2013), Identifiability of transient storage model parameters along a mountain stream, *Water Resour. Res.*, *49*, 5290–5306, doi:10.1002/wrcr.20413.
Kerr, P. C., M. N. Gooseff, and D. Bolster (2013), The significance of model structure in one-dimensional stream solute transport models with multiple transient storage zones—Competing vs. nested arrangements, *Remote Sens. Environ.*, *497*, 133–144, doi:10.1016/j.jhydrol. 2013.05.013.
Kim, M., L. Pangle, C. Cardoso, M. Lora, T. Volkmann, Y. Wang, C. Harman, and P. Troch (2016), Transit time distributions and StorAge Selection functions in a variably-saturated sloping soil lysimeter: Direct observation of internal and external transport variability, *Water Resour. Res.*, doi:10.1002/2016WR018620, in press.
Kirchner, J. W., X. Feng, and C. Neal (2000), Fractal stream chemistry and its implications for contaminant transport in catchments, *Nature*, *403*(6769), 524–527, doi:10.1038/35000537.
Leopold, L. B., and T. Maddock (1953), The hydraulic geometry of stream channels and some physiographic implications, technical report, *U.S. Dep. of the Inter., U.S. Geol. Surv.* Geological Survey Professional Paper 252, United States Government Printing Office, Washington, D. C.
Loheide, S. P., and J. D. Lundquist (2009), Snowmelt-induced diel fluxes through the hyporheic zone, *Water Resour. Res.*, *45*, W07404, doi:10.1029/2008WR007329.
Malzone, J. M., and C. S. Lowry (2014), Focused groundwater controlled feedbacks into the hyporheic zone during baseflow recession, *Ground Water*, *53*(2), 217–226, doi:10.1111/gwat.12186.
Payn, R. A., M. N. Gooseff, B. L. McGlynn, K. E. Bencala, and S. M. Wondzell (2009), Channel water balance and exchange with subsurface flow along a mountain headwater stream in Montana, United States, *Water Resour. Res.*, *45*, W11427, doi:10.1029/2008WR007644.
Rinaldo, A., K. J. Beven, E. Bertuzzo, L. Nicotina, J. Davies, A. Fiori, D. Russo, and G. Botter (2011), Catchment travel time distributions and water flow in soils, *Water Resour. Res.*, *47*, W07537, doi:10.1029/2011WR010478.
Rinaldo, A., P. Benettin, C. J. Harman, M. Hrachowitz, K. J. McGuire, Y. van der Velde, E. Bertuzzo, and G. Botter (2015), Storage selection functions: A coherent framework for quantifying how catchments store and release water and solutes, *Water Resour. Res.*, *51*, 4840–4847, doi:10.1002/2015WR017273.
Rodhe, A., L. Nyberg, and K. Bishop (1996), Transit times for water in a small till catchment from a step shift in the oxygen 18 content of the water input, *Water Resour. Res.*, *32*(12), 3497–3511, doi:10.1029/95WR01806.
Runkel, R. L., D. M. McKnight, and E. D. Andrews (1998), Analysis of transient storage subject to unsteady flow: Diel flow variation in an Antarctic stream, *J. North Am. Benthol. Soc.*, *17*(2), 143–154.
Sawyer, A. H., and M. B. Cardenas (2009), Impact of dam operations on hyporheic exchange in the riparian zone of a regulated river, *Hydrol. Processes*, *23*, 2129–2137, doi:10.1002/hyp.7324.
Sawyer, A. H., F. Shi, J. T. Kirby, and H. A. Michael (2013), Dynamic response of surface water-groundwater exchange to currents, tides, and waves in a shallow estuary, *J. Geophys. Res. Oceans*, *118*, 1749–1758, doi:10.1002/jgrc.20154.
Schmadel, N. M., et al. (2016), Stream solute tracer timescales changing with discharge and reach length confound process interpretation, *Water Resour. Res.*, *52*, 3227–3245, doi:10.1002/2015WR018062.
Stanford, J. A., and J. V. Ward (1993), An ecosystem perspective of alluvial rivers: Connectivity and the hyporheic corridor, *J. North Am. Benthol. Soc.*, *12*(1), 48–60.
Storey, R. G., K. W. F. Howard, and D. D. Williams (2003), Factors controlling riffle-scale hyporheic exchange flows and their seasonal changes in a gaining stream: A three-dimensional groundwater flow model, *Water Resour. Res.*, *39*(2), 1034, doi:10.1029/2002WR001367.
Swanson, F. J., and M. E. James (1975), Geology and geomorphology of the H.J. Andrews Experimental Forest, western Cascades, *Oregon, technical report* USDA For. Ser. PNW-188, 14 pp., Pacific Northwest Forest and Range Experiment Station, Portland, Oreg.
Swanson, F. J., and J. A. Jones (2002), Geomorphology and hydrology of the HJ Andrews experimental forest, Blue River, Oregon, in *Field Guide to Geologic Processes in Cascadia: Field Trips to Accompany the 98th Annual Meeting of the Cordilleran Section of the Geological Society of America*, vol. 36, edited by G. W. Moore, pp. 289–314, Oregon Department of Geology and Mineral Industries, Portland, Oreg.
van der Velde, Y., P. J. J. F. Torfs, S. E. A. T. M. van der Zee, and R. Uijlenhoet (2012), Quantifying catchment-scale mixing and its effect on time-varying travel time distributions, *Water Resour. Res.*, *48*, W06536, doi:10.1029/2011WR011310.
Vannote, R. L., G. W. Minshall, K. W. Cummins, J. R. Sedell, and C. E. Cushing (1980), The river continuum concept, *Can. J. Fish. Aquat. Sci.*, *37*, 130–137.
Voltz, T., M. N. Gooseff, A. S. Ward, K. Singha, M. Fitzgerald, and T. Wagener (2013), Riparian hydraulic gradient and stream-groundwater exchange dynamics in steep headwater valleys, *J. Geophys. Res. Earth Surf.*, *118*, 953–969, doi:10.1002/jgrf.20074.
Wagner, B. J., and J. W. Harvey (1997), Experimental design for estimating parameters of rate-limited mass transfer: Analysis of stream tracer studies, *Water Resour. Res.*, *33*(7), 1731–1741, doi:10.1029/97WR01067.
Ward, A. S., M. Fitzgerald, M. N. Gooseff, T. J. Voltz, A. M. Binley, and K. Singha (2012), Hydrologic and geomorphic controls on hyporheic exchange during base flow recession in a headwater mountain stream, *Water Resour. Res.*, *48*, W04513, doi:10.1029/2011WR011461.
Ward, A. S., M. N. Gooseff, T. J. Voltz, M. Fitzgerald, K. Singha, and J. P. Zarnetske (2013a), How does rapidly changing discharge during storm events affect transient storage and channel water balance in a headwater mountain stream?, *Water Resour. Res.*, *49*, 5473–5486, doi:10.1002/wrcr.20434.
Ward, A. S., R. A. Payn, M. N. Gooseff, B. L. McGlynn, K. E. Bencala, C. A. Kelleher, S. M. Wondzell, and T. Wagener (2013b), Variations in surface water-ground water interactions along a headwater mountain stream: Comparisons between transient storage and water balance analyses, *Water Resour. Res.*, *49*, 3359–3374, doi:10.1002/wrcr.20148.
Ward, A. S., N. M. Schmadel, S. M. Wondzell, C. J. Harman, M. N. Gooseff, and K. Singha (2016), Hydrogeomorphic controls on hyporheic and riparian transport in two headwater mountain streams during base flow recession, *Water Resour. Res.*, *52*, 1479–1497, doi:10.1002/2015WR018225.

Wondzell, S. M. (2006), Effect of morphology and discharge on hyporheic exchange flows in two small streams in the Cascade Mountains of Oregon, USA, *Hydrol. Processes*, *20*(2), 267–287, doi:10.1002/hyp.5902.

Wondzell, S. M., M. N. Gooseff, and B. L. McGlynn (2007), Flow velocity and the hydrologic behavior of streams during baseflow, *Geophys. Res. Lett.*, *34*, L24404, doi:10.1029/2007GL031256.

Wondzell, S. M., M. N. Gooseff, and B. L. McGlynn (2009a), An analysis of alternative conceptual models relating hyporheic exchange flow to diel fluctuations in discharge during baseflow recession, *Hydrol. Processes*, *24*(6), 686–694, doi:10.1002/hyp.7507.

Wondzell, S. M., J. LaNier, and R. Haggerty (2009b), Evaluation of alternative groundwater flow models for simulating hyporheic exchange in a small mountain stream, *J. Hydrol.*, *364*(1–2), 142–151, doi:10.1016/j.jhydrol.2008.10.011.

Worman, A., A. I. Packman, H. Johansson, and K. Jonsson (2002), Effect of flow-induced exchange in hyporheic zones on longitudinal transport of solutes in streams and rivers, *Water Resour. Res.*, *38*(1), doi:10.1029/2001WR000769.